Flat Band and η-Pairing States in a One-Dimensional Moiré Hubbard Model

R. Wang(王冉)[1] and Z. Song(宋智)[2*]

[1]*College of Physics and Materials Science, Tianjin Normal University, Tianjin 300387, China*
[2]*School of Physics, Nankai University, Tianjin 300071, China*

(Received 27 October 2023; accepted manuscript online 11 March 2024)

A Moiré system is formed when two periodic structures have a slightly mismatched period, resulting in unusual strongly correlated states in the presence of particle-particle interactions. The periodic structures can arise from the intrinsic crystalline order and periodic external field. We investigate a one-dimensional Hubbard model with periodic on-site potential of period n_0, which is commensurate to the lattice constant. For large n_0, the exact solution demonstrates that there is a midgap flat band with zero energy in the absence of Hubbard interaction. Each Moiré unit cell contributes two zero energy levels to the flat band. In the presence of Hubbard interaction, the midgap physics is demonstrated to be well described by a uniform Hubbard chain in which the effective hopping and on-site interaction strength can be controlled by the amplitude and period of the external field. Numerical simulations are performed to demonstrate the correlated behaviors in the finite-sized Moiré Hubbard system, including the existence of an η-pairing state and bound pair oscillation. This finding provides a method to enhance the correlated effect by a spatially periodic external field.

DOI: 10.1088/0256-307X/41/4/047101

The theoretical and experimental studies on twisted bilayer graphene (TBG) indicate that the interplay of lattice geometry and many-body interactions can induce exotic quantum states,[1–11] which include superconducting and correlated insulating behavior. In general, these phenomena are known to arise from formation of a flat band with low energy and narrow bandwidth, which greatly enhances the electronic interaction effect. The flat bands are connected to the p-wave superconductor Kitaev model with rich topological properties.[12–16] However, it is slightly difficult to observe these interesting correlation-induced phenomena because an accurate magic angle in TBG causes constraints in device fabrication. Therefore, it is natural to look for a one-dimensional version of TBG, providing easier access to the flat band by alternative approaches. A starting point is Moiré patterns, which emerge due to the superposition of two periodic structures, with either slightly different periods or different orientations. Such patterns have been realized in materials.[17–23]

In principle, a one-dimensional Moiré system can be deliberately engineered as a super-long-period system when the periods of two ingredients are slightly different but commensurate.[24–26] It is essentially a one-dimensional periodic system with a large unit cell, which may result in weak inter-unit-cell coupling, or a nearly flat band. Theoretically, two periodic structures can arise from the intrinsic crystalline order and periodic external field. In condensed matter, particles are usually confined by a periodic potential in synthetic and natural materials. Another periodic structure can come from another external field. Compared to the magic angle in TBG, the amplitude and period of a periodic external field may be easy to control in experiments.

In this Letter, we investigate a Moiré Hubbard model which is a uniform Hubbard chain subjected to a field by cosinusoidal modulation with a period commensurate to the lattice constant. In the absence of the Hubbard interaction, a midgap flat band is induced by the periodic field when the field amplitude or the superlattice unit cell is large enough. We determine that the corresponding eigen wave functions are Gaussian-like with their centers located at each zero potential point. When the field strength or unit cell decreases, the flat band becomes a narrow band, which can be well characterized by tight-binding approximation, i.e., the Gaussian-like wave functions playing the role of Wannier functions. In the presence of the Hubbard interaction, the Moiré pattern physics is demonstrated to be well described by a uniform Hubbard chain with effective hopping (J_{eff}) and on-site interaction strength (U_{eff}). Importantly, the ratio $U_{\text{eff}}/J_{\text{eff}}$ can be controlled by the amplitude and period of the external field to achieve the goal of enhancing the electronic interaction effect. Numerical simulations are performed to demonstrate the correlated behaviors of an ordinary Hubbard model in the finite-sized Moiré Hubbard system. The first one is the existence of η-pairing state, which is believed to be a possible mechanism of superconductivity based on the concept of off-diagonal long-range order (ODLRO). The other is bound pair oscillation, demonstrating correlated dynamics. This finding provides a theoretical model as a one-dimensional analogue of twisted bilayer graphene. The advantage of this method is that the correlated effect can be enhanced by the external field. We expect that our results will benefit experimental research.

In the following, first we present the one-dimensional Hubbard model with spatially modulated on-site potential. Then, we discuss midgap physics in the model. We propose a dynamic scheme to experimentally demonstrate that the Moiré Hubbard model supports midgap bound-pair states. Finally, we provide a summary.

*Corresponding author. Email: songtc@nankai.edu.cn
© 2024 Chinese Physical Society and IOP Publishing Ltd

Model Hamiltonian. We consider a one-dimensional Hubbard model with spatially modulated on-site potential:

$$H = H_0 + U\sum_j n_{j,\uparrow}n_{j,\downarrow} \tag{1}$$

with

$$H_0 = \sum_{j,\sigma=\uparrow,\downarrow}\Big[-\kappa c^\dagger_{j,\sigma}c_{j+1,\sigma} + \text{H.c.} + (-1)^j V \times \cos\Big(\frac{\pi j}{n_0}\Big)n_{j,\sigma}\Big], \tag{2}$$

where $c_{j,\sigma}$ ($c^\dagger_{j,\sigma}$) is the annihilation (creation) operator for an electron at site j with spin σ and $n_{j,\sigma} = c^\dagger_{j,\sigma}c_{j,\sigma}$. We schematically illustrate that such a potential can be realized by a continuous potential of trigonometric function (see Fig. 1). H is known as a one-dimensional standard Hubbard model with the uniform case ($V = 0$), which has been studied in many perspectives.[27,28] However, this work investigates the effect of nonzero V on the property of the Hubbard model. Parameters κ and U play the role of a kinetic and interaction energy scale, respectively. The on-site staggered potential is commensurate for integer n_0, which determines the Morié period $2n_0$. We consider a ring lattice of length $N = 2Mn_0$ and take $c_{N+1,\sigma} \equiv c_{1,\sigma}$ to impose a periodic boundary condition. The main results of this work are independent of the boundary conditions.

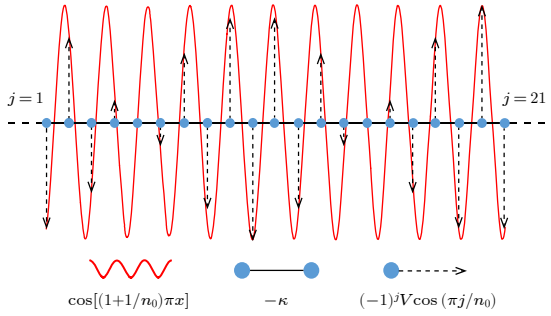

Fig. 1. Schematic illustration of a one-dimensional Moiré system consisting of two periodic ingredients with different but commensurate periods. The lattice (array of solid blue circles) constant is 1, while the external field (red line) is cosinusoidal function $\cos[(1+1/n_0)\pi x]$ with period $2/(1+1/n_0)$. The whole system is still periodic with a long period $2n_0$ for large n_0. The dotted arrow denotes the on-site potential distribution on the lattice, which is spatially modulated and staggered as $(-1)^j\cos(\pi j/n_0)$ in Eq. (2). Here, $j = \text{INT}(x)$ is the integer portion of the coordinate x, $-\kappa$ is the nearest-neighbor hopping strength, and $n_0 = 10$.

We focus on the interaction-free case with zero U and rewrite H_0 in the form of

$$H_0 = \sum_{m=1}^{M}\Big[\sum_{l=1}^{2n_0-1}(-\kappa)(c^\dagger_{m,l}c_{m,l+1} + c^\dagger_{m,2n_0}c_{m+1,1} + \text{H.c.}) + \sum_{l=1}^{2n_0}(-1)^l V\cos\Big(\frac{\pi l}{n_0}\Big)n_{m,l}\Big]. \tag{3}$$

Here we neglect the index of σ, with the mapping $c_{2(m-1)n_0+l,\sigma} = c_{m,l}$ and $n_{m,l} = c^\dagger_{m,l}c_{m,l}$; index m denotes the unit cell, and l denotes the position of the site in the m-th unit cell. We impose the periodic boundary condition $c_{M+1,1} = c_{1,1}$ and perform the Fourier transformations

$$c_{m,l} = \frac{1}{\sqrt{M}}\sum_k e^{ikm}c_{k,l}, \tag{4}$$

with $k = 2n\pi/M$, $n = 0, 1, \ldots, M-1$. Therefore, the transformation block diagonalizes the Hamiltonian with translational symmetry, that is, H_0 can be written as a block-diagonal form:

$$H_0 = \sum_k H_{0k} = \sum_k \psi^\dagger_k h_{0k}\psi_k, \tag{5}$$

satisfying $[H_{0k}, H_{0k'}] = 0$, in which the operator vector is

$$\psi_k = (c_{k,1}, c_{k,2}, \ldots, c_{k,2n_0})^{\mathrm{T}}, \tag{6}$$

and h_{0k} is a $2n_0 \times 2n_0$ matrix

$$h_{0k} = \begin{pmatrix} A_1 & -\kappa & 0 & \cdots & & & -\kappa e^{-ik} \\ -\kappa & A_2 & -\kappa & 0 & \cdots & & \\ 0 & -\kappa & A_3 & -\kappa & 0 & \cdots & \\ \vdots & 0 & -\kappa & \ddots & & & \\ & \vdots & 0 & & & & \\ & & \vdots & & \ddots & -\kappa & \\ -\kappa e^{ik} & & & & -\kappa & A_{2n_0} & \end{pmatrix} \tag{7}$$

with $A_l = (-1)^l V\cos(\pi l/n_0)$. Matrix h_{0k} corresponds to a uniformly hopping ring with non-uniform on-site potential and a threading flux k through it. The flux can be neglected in large n_0 limit. The system then has approximate reflection symmetry about the site n_0 due to the fact that $A_{2n_0-l} = A_l$. The eigenvector of h_{0k} has the form of

$$\varphi_0(k, n) = \sum_l^{2n_0} f^n_{k,l}c^\dagger_{k,l}|0\rangle, \tag{8}$$

where $n = 1, 2, \ldots, 2n_0$ denotes the energy level index $E_{0k}(n)$; $|0\rangle$ is the vacuum state for the creation fermion operator $c^\dagger_{k,l}$. The exact solution of $\{f^n_{k,l}\}$ is difficult to obtain. However, there are M pairs of zero potential points at $(m, l) = (m, n_0/2)$ and $(m, 3n_0/2)$ [or $j = 2n_0(m-1)+n_0/2$ and $2n_0(m-1)+3n_0/2$ for the original coordinate] in the limit case with $n_0 \gg 1$ and nonzero V. In the following, we will demonstrate that there are M pairs of zero energy eigenvectors.

As an approximation, we take a linearization of the Hamiltonian as an effective Hamiltonian by Taylor expansion of the potential around each zero potential point. Defining Λ as the range of validity for this linearization approximation, we write the linearized effective Hamiltonian in the form of

$$H^{\text{eff}}_0 = \sum_k (H^+_{0k} + H^-_{0k}), \tag{9}$$

where

$$H^\pm_{0k} = \sum_{l=n_0\pm n_0/2-\Lambda}^{n_0\pm n_0/2+\Lambda}\Big[-\kappa c^\dagger_{k,l}c_{k,l+1} + \text{H.c.} \mp (-1)^l V \times (\pi \pm \pi/2 - \frac{\pi l}{n_0})n_{k,l}\Big]. \tag{10}$$

We determine that H^{eff}_0 has reflection symmetry about the point $l = n_0$, as mentioned regarding the approximate

symmetry of h_{0k}. Introducing a set of operators defined by

$$\phi_{\pm}^{\dagger}(k)=\sum_{l=n_0\pm n_0/2-\Lambda}^{n_0\pm n_0/2+\Lambda} a_{l,\pm}c_{k,l}^{\dagger}, \tag{11}$$

where

$$a_{l,\pm}=\Big(\frac{V}{2\kappa n_0}\Big)^{1/4}\sin[(1+2l)\pi/4]e^{-\frac{V\pi}{4\kappa n_0}[l-(n_0\pm n_0/2)]^2}. \tag{12}$$

A straightforward derivation demonstrates

$$[H_0^{\rm eff},\,\phi_{\pm}^{\dagger}(k)]=\sum_{l=n_0\pm n_0/2-\Lambda}^{n_0\pm n_0/2+\Lambda}[(-\kappa)(a_{l+1,\pm}+a_{l-1,\pm}) \mp(-1)^l V(\pi\pm\pi/2-\frac{\pi l}{n_0})a_{l,\pm}]c_{k,l}^{\dagger}. \tag{13}$$

In the $\frac{V\pi}{4\kappa n_0}\to 0$ limit, the above equation can be rewritten as

$$\begin{aligned}&[H_0^{\rm eff},\,\phi_{\pm}^{\dagger}(k)]\\ &\approx\Big(\frac{V}{2\kappa n_0}\Big)^{1/4}\sum_{l=n_0\pm n_0/2-\Lambda}^{n_0\pm n_0/2+\Lambda}V\Big[\frac{\pi l}{n_0}-(\pi\pm\pi/2)\Big]\\ &\quad\times\{\cos[(1+2l)\pi/4]\pm(-1)^l\sin[(1+2l)\pi/4]\}\\ &\quad\times e^{-\frac{V\pi}{4\kappa n_0}[l-(n_0\pm n_0/2)]^2}c_{k,l}^{\dagger}.\end{aligned} \tag{14}$$

We would like to point out that the coefficient always satisfies

$$\cos[(1+2l)\pi/4]-(-1)^l\sin[(1+2l)\pi/4]=0, \tag{15}$$

$$\cos[(1+2l)\pi/4]+(-1)^l\sin[(1+2l)\pi/4]=0, \tag{16}$$

under conditions $l\in[n_0/2-\Lambda,\,n_0/2+\Lambda]$ and $l\in[3n_0/2-\Lambda,\,3n_0/2+\Lambda]$, respectively. Thus, we have

$$[H_0^{\rm eff},\phi_{\pm}^{\dagger}(k)]\approx 0. \tag{17}$$

It approximately indicates that a set of states $\phi_{\pm}^{\dagger}(k)|0\rangle$ are eigenstates of $H_0^{\rm eff}$ with zero energy. Similarly, a set of local Gaussian wavepackets $\phi_{\pm}^{\dagger}(m)|0\rangle$ with

$$\begin{aligned}\phi_{\pm}^{\dagger}(m)=\Big(\frac{V}{2\kappa n_0}\Big)^{1/4}&\sum_{l=n_0\pm n_0/2-\Lambda}^{n_0\pm n_0/2+\Lambda}\sin[(1+2l)\pi/4]\\ &\times e^{-\frac{V\pi}{4\kappa n_0}[l-(n_0\pm n_0/2)]^2}e^{ikm}c_{m,l}^{\dagger}\end{aligned} \tag{18}$$

are eigenstates of $H_0^{\rm eff}$ with zero energy, where $|0\rangle$ is the vacuum state for the creation fermion operator $c_{m,\,l}^{\dagger}$. It is easy to check that there are a total of $2M$ zero energy eigenvectors.

Eigenvector $\varphi_0(k,\,n)$ and spectrum $E_{0k}(n)$ can be obtained numerically by exact diagonalization of the matrix h_{0k} in the case of finite n_0 limit. We plot the profiles of the wave function and the spectrum for three representative cases (see Fig. 2).

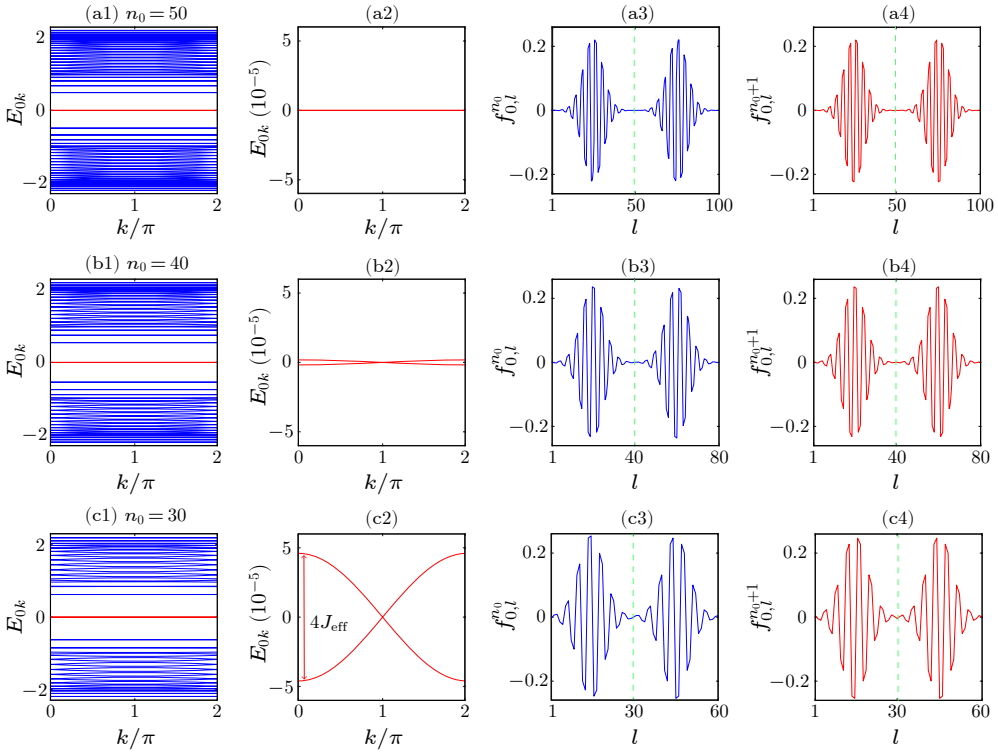

Fig. 2. Plots of energy spectra (a1)–(c1) and selected midgap wave functions (a3)–(c3) and (a4)–(c4), obtained from the exact diagonalization of the matrix in Eq. (7) for fixed V and three typical $n_0=50$, 40, and 30, respectively. (a2)–(c2) The zoomed-in version of (a1)–(c1), selecting typical energy levels around zero energy. We only plot the wave functions in a single unit cell with $k=0$. It is determined that the zero energy states are antisymmetric (blue) and symmetric (red) about the point $l=n_0$ (green dotted line), which accords with the fact that $H_0^{\rm eff}$ in Eq. (9) has reflection symmetry. As n_0 decreases, the width of the wavepackets increases and the overlap between two neighbor ones appears. Meanwhile, the midgap flat band becomes a midgap narrow band. The energy unit is κ. The system parameters are $\kappa=V=1$ and $M=100$.

We determine that for sufficiently large n_0, the zero energy states are separated Gaussian wavepackets, which accords with our above analysis. As n_0 decreases, the width of the wavepackets increases and the overlap between two neighbor ones appears. Moreover, the midgap flat band becomes a midgap narrow band. Similar things happen when n_0 is fixed and V is varied: there is a midgap flat band in large V limit with $V \gg \kappa$ because every zero potential site decouples from the neighbors. Extreme localized states (site state) form at each zero potential point. As V decreases, the site state becomes a wavepacket, and as its width increases, the overlap between two neighbor ones appears. Each zero potential point becomes the center of the wavepackets. Moreover, the midgap flat band becomes a midgap narrow band. This process is demonstrated by numerical simulation in Fig. 3.

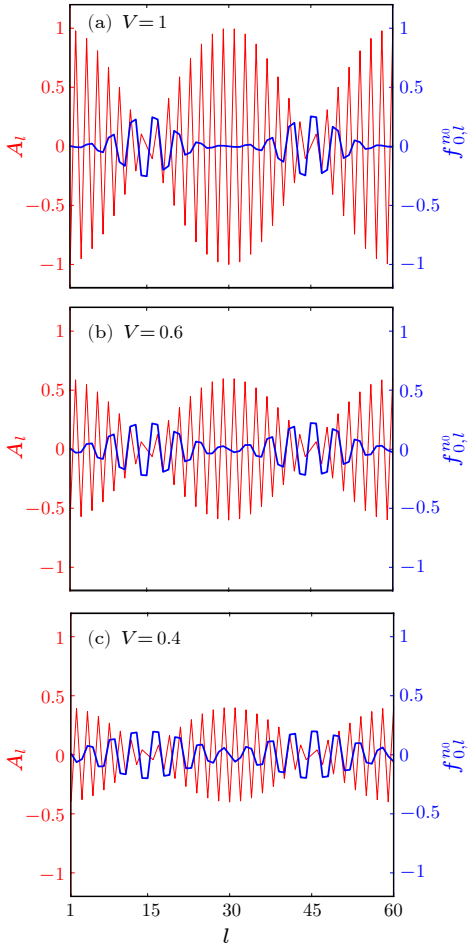

Fig. 3. Profiles of wave functions (blue) in the midgap and on-site potential distribution A_l (red). Three representative values of V are selected and the corresponding wave functions $f^n_{k,\,l}$ with $k=0$ are obtained by exact diagonalization of the matrix in Eq. (7). As is expected, we can see that the wave functions are Gaussian-like with the center being localized around zero potential points. The width of the wavepackets increases and the overlap between two neighbor ones appears as V decreases. The system parameters are $\kappa=1$ and $n_0=30$.

It is clear that this Moiré system can be regarded as a superlattice: $\phi_\pm(m)$ $[\phi^\dagger_\pm(m)]$ annihilates (creates) a localized Wannier state at superlattice site m. The midgap band is depicted by tight-binding Hamiltonian

$$H_0^{\rm MG} = J_{\rm eff}\sum_m \left[\phi^\dagger_+(m)\phi_-(m)+\phi^\dagger_+(m)\phi_-(m+1)+{\rm H.c.}\right]. \tag{19}$$

The hopping constant $J_{\rm eff}$ can be estimated from the numerical result for the width $(4J_{\rm eff})$ of the midgap narrow band, as indicated in Fig. 2(c2). When we fix n_0 and increase V, every two $\phi^\dagger_\pm(k)$ have less overlap, and the corresponding energy levels become degenerate. The parameter $J_{\rm eff}$ is determined by the energy level difference. We determine that $J_{\rm eff}$ decreases as V increases. We would like to point out that, unlike the usual single lowest band approximation, $J_{\rm eff}$ is always positive since $H_0^{\rm MG}$ describes a midgap band, and does not violate the node theorem for the eigen wave function in a one-dimensional system.

Midgap Hubbard Model. So far we have established the tight binding description of the midgap physics for the Moiré system. In the following, we will consider the case with nonzero U. $H_0^{\rm MG}$ then can be modified by adding the spin index, replacing $\phi_\pm(m)$ by $\phi_{\pm,\,\sigma}(m)$. The above analysis still holds for interaction-free terms $(H^{\rm MG}_{0,\,\sigma})$. The midgap Hubbard model Hamiltonian reads

$$H^{\rm MG} = \sum_{\sigma=\uparrow,\downarrow} H^{\rm MG}_{0,\sigma} + U_{\rm eff}\sum_{m,\rho=\pm}\phi^\dagger_{\rho,\uparrow}(m)\phi_{\rho,\uparrow}(m) \times \phi^\dagger_{\rho,\downarrow}(m)\phi_{\rho,\downarrow}(m), \tag{20}$$

where $H^{\rm MG}_{0,\,\sigma}$ is extended from $H_0^{\rm MG}$, which has the form of

$$H^{\rm MG}_{0,\sigma} = J_{\rm eff}\sum_m[\phi^\dagger_{+,\,\sigma}(m)\phi_{-,\sigma}(m) + \phi^\dagger_{+,\sigma}(m)\phi_{-,\sigma}(m+1)+{\rm H.c.}]. \tag{21}$$

The effective Hubbard interaction strength $U_{\rm eff}$ is determined by

$$U_{\rm eff} = U\langle 0|\phi_{\rho,\downarrow}(m)\phi_{\rho,\uparrow}(m)[\sum_l(n_{m,\,l,\uparrow}n_{m,\,l,\downarrow})] \times \phi^\dagger_{\rho,\uparrow}(m)\phi^\dagger_{\rho,\downarrow}(m)|0\rangle, \tag{22}$$

which can be estimated by numerical computation. We would like to point out that Eq. (22) also indicates the degree of localization of the wavefunction $\phi_{\rho,\,\uparrow}$ $(\phi_{\rho,\,\downarrow})$. As $\phi_{\rho,\,\uparrow}$ $(\phi_{\rho,\,\downarrow})$ becomes more local, $U_{\rm eff}$ increases, so we determine that $U_{\rm eff}$ increases as V increases. We plot the profiles of the two-particle eigenstates and the spectrum for three representative cases (see Fig. 4). We determine that for sufficiently large n_0, the flat band separates into two flat bands, one is a pair-band, the other is a scattering band. The width of the two bands increases as n_0 decreases.

To verify the tight-binding approximation, one can fit the result from exact diagonalization for the original Moiré Hamiltonian by that of $H^{\rm MG}$. We consider a system with double Moiré unit cells,

$$H_{M2} = \sum_{j=1,\sigma=\uparrow,\downarrow}^{4n_0}\Big[-\kappa c^\dagger_{j,\,\sigma}c_{j+1,\,\sigma}+{\rm H.c.}+(-1)^jV \times\cos\Big(\frac{\pi j}{n_0}\Big)n_{j,\sigma}\Big]+U\sum_{j=1}^{4n_0}n_{j,\uparrow}n_{j,\downarrow}, \tag{23}$$

which corresponds to a four-site Hubbard ring.

In addition to Eq. (22), $U_{\rm eff}$ can further be obtained by fitting the energy levels of H_{M2} to that of $H^{\rm MG}$. The fitting results are given in Figs. 4(a1)–4(c1), and the obtained $U_{\rm eff}$ by fitting is compared with the value estimated from Eq. (22). We determine that the approximation works quite well. Furthermore, the bound-pair levels [upper band in Fig. 4(a1)–4(c1)] accords with the analytical expression

$$\varepsilon_\mu = \sqrt{U_{\rm eff}^2 + 16J_{\rm eff}^2 \cos^2\left(\frac{\mu\pi}{M}\right)} \tag{24}$$

with $\mu = 0, 1, \ldots, 2M-1$, which has been obtained in previous works.[29,30]

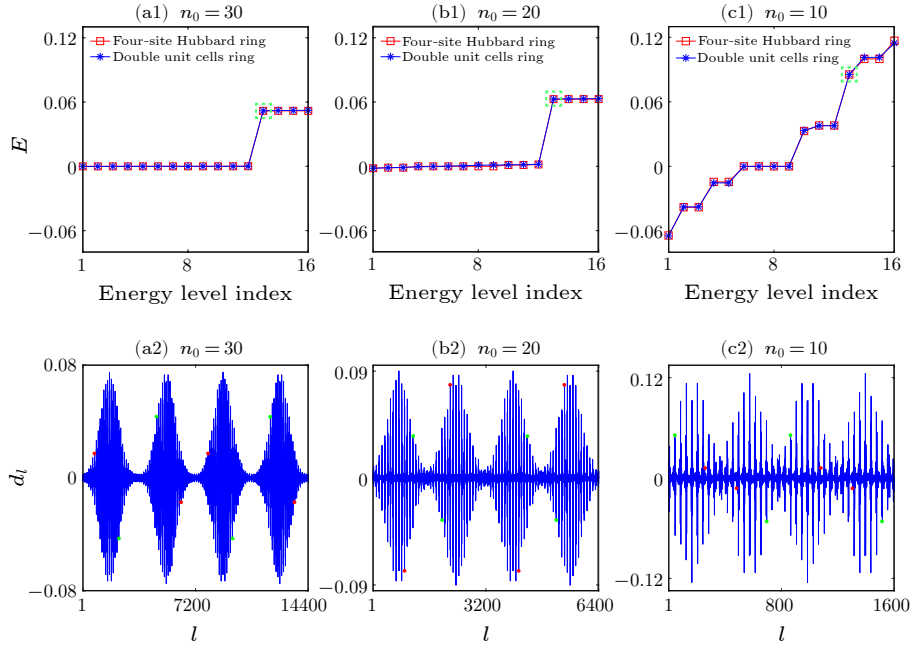

Fig. 4. Comparison of the midgap states of the Moiré Hubbard model and its tight-binding description. (a1)–(c1) Plots of midgap energy levels (blue star) obtained by exact diagonalization of the Hamiltonian in Eq. (23) for three typical n_0. The red squares represent the energy levels of a four-site Hubbard ring with fitting values of $J_{\rm eff}$ and $U_{\rm eff}$. We can find that for sufficiently large n_0, the original single flat band ($U = 0$) separates into two flat bands (a1), the upper band is the pair band. As n_0 decreases, the width of the two bands increases [(b1) and (c1)]. The pair band is fitted by the numerical result from the four-site Hubbard ring in Eq. (20). The fitting parameters of the four-site Hubbard ring are $J_{\rm eff} = 2.30 \times 10^{-5}$, $U_{\rm eff} = 5.18 \times 10^{-2}$ (5.11×10^{-2}) in (a1), $J_{\rm eff} = 6.20 \times 10^{-4}$, $U_{\rm eff} = 6.27 \times 10^{-2}$ (6.14×10^{-2}) in (b1), and $J_{\rm eff} = 1.90 \times 10^{-2}$, $U_{\rm eff} = 8.54 \times 10^{-2}$ (8.42×10^{-2}) in (c1), respectively. Here the values of $U_{\rm eff}$ in each bracket are obtained from Eq. (22). (a2)–(c2) Plots of the eigen wave function d_l of the lowest energy level, i.e., $E = U_{\rm eff}$ (green dashed box) at the upper band. It is the η-pairing state, which obeys the relation in Eq. (33) as expected, indicated by two groups of red and green solid circles. The results demonstrate that the tight-binding approximation works quite well and there exists η-pairing states in the superlattice near the Fermi level. The system parameters are $\kappa = 1$, $V = 1$, and $U = 0.5$.

In particular, when taking $\mu = M/2$, we have $\varepsilon_{M/2} = U_{\rm eff}$, which is the lowest bound-pair energy level. The corresponding eigenstate is

$$|\Psi_\eta^1\rangle = \eta|0\rangle, \tag{25}$$

where η is the so-called η-pairing operator defined as

$$\eta = \frac{1}{\sqrt{2M}} \sum_{m=1,\rho=\pm}^{M} \rho\phi_{\rho,\uparrow}^\dagger(m)\phi_{\rho,\downarrow}^\dagger(m). \tag{26}$$

According to the seminal work by Yang,[31] we have

$$[H^{\rm MG}, \eta] = U_{\rm eff}\eta, \tag{27}$$

which ensures

$$H^{\rm MG}|\Psi_\eta^\mu\rangle = \mu U_{\rm eff}|\Psi_\eta^\mu\rangle, \tag{28}$$

i.e., state

$$|\Psi_\eta^\mu\rangle = \eta^\mu|0\rangle \tag{29}$$

is the eigenstate of $H^{\rm MG}$ with energy $\mu U_{\rm eff}$. The η-pairing state $|\Psi_\eta^\mu\rangle$ has been demonstrated to have ODLRO if μ/M is finite ($0 < \mu/M < 1$) in the thermodynamic limit, $M \to \infty$.

In general, a complete set basis of the two-electron subspace $\{|l\rangle\}$ is

$$|l\rangle = c_{i,\uparrow}^\dagger c_{j,\downarrow}^\dagger|0\rangle, \tag{30}$$

where l is defined as $l = 2Mn_0(i-1) + j$, with $i, j \in [1, 2Mn_0]$. Any two-electron state with opposite spins can then be expressed in the form of

$$|\Psi\rangle = \sum_l d_l|l\rangle. \tag{31}$$

For a small-size Moiré Hubbard model H_{M2} with a pair of electrons, the corresponding η-pairing state is

$$|\Psi_\eta^1\rangle = \frac{1}{2}\sum_{\rho=\pm}\rho[\phi_{\rho,\uparrow}^\dagger(1)\phi_{\rho,\downarrow}^\dagger(1) + \phi_{\rho,\uparrow}^\dagger(2)\phi_{\rho,\downarrow}^\dagger(2)]|0\rangle, \tag{32}$$

which requires that the eigen wave function with energy $U_{\rm eff}$ satisfies the relation

$$d_l = -d_{4(Mn_0)^2-l},\ d_l = d_{l+2(Mn_0)^2},\quad l \in [1,\ 2(Mn_0)^2]. \tag{33}$$

The numerical results for the eigen wave function plotted in Fig. 4(a2)–4(c2) accord with this analysis. Taking the numerical single-particle wavefunctions of $\phi^\dagger_{\rho,\uparrow}$ ($\phi^\dagger_{\rho,\downarrow}$) into Eq. (32), the overlaps between the wavefunction expression of Eq. (32) and the wavefunctions of Fig. 4(a2)–4(c2) are 91.46%, 91.45%, and 90.66%, respectively. These findings demonstrate that midgap physics for the Hubbard Moiré system can be well captured by a simple Hubbard model. The advantage of this system is evident: the parameters $J_{\rm eff}$ and $U_{\rm eff}$ can be controlled by the external field, similar to what happens in the optical lattice system. Moreover, the midgap Hubbard model provides the possibility of realizing a one-dimensional superconducting state based on the formation of η pairs near the Fermi level.

Bound-Pair Dynamics. The above analysis indicates that the Moiré Hubbard model supports midgap bound-pair states, which are protected from thermal fluctuation due to the energy gap. This may be allowed to observe the related dynamics in experiment, similar to the Bloch oscillation.[32] To verify and demonstrate such a prediction, we consider a simple case consisting of a single Moiré unit cell and investigate the dynamics of the system with specific parameters.

The corresponding tight-binding Hamiltonian reads

$$H_1^{\rm MG} = J_{\rm eff}[\phi^\dagger_+(1)\phi_-(1) + {\rm H.c.}] + U_{\rm eff} \times \sum_{\rho=\pm} \phi^\dagger_{\rho,\uparrow}(1)\phi_{\rho,\uparrow}(1)\phi^\dagger_{\rho,\downarrow}(1)\phi_{\rho,\downarrow}(1), \tag{34}$$

which is a two-site Hubbard model. In the two-particle invariant subspace, spanned by a two-particle basis

$$\begin{aligned} &\phi^\dagger_{+,\uparrow}(1)\phi^\dagger_{+,\downarrow}(1)|0\rangle,\quad \phi^\dagger_{-,\uparrow}(1)\phi^\dagger_{-,\downarrow}(1)|0\rangle,\\ &\phi^\dagger_{+,\uparrow}(1)\phi^\dagger_{-,\downarrow}(1)|0\rangle,\quad \phi^\dagger_{-,\uparrow}(1)\phi^\dagger_{+,\downarrow}(1)|0\rangle, \end{aligned} \tag{35}$$

the matrix representation of $H_1^{\rm MG}$ is

$$h_1 = J_{\rm eff}\begin{pmatrix} U_{\rm eff}/J_{\rm eff} & 0 & 1 & 1\\ 0 & U_{\rm eff}/J_{\rm eff} & 1 & 1\\ 1 & 1 & 0 & 0\\ 1 & 1 & 0 & 0 \end{pmatrix}, \tag{36}$$

which has parity symmetry, i.e., $Ph_1P^{-1} = h_1$. The reflectional operator P is defined as $P\phi^\dagger_{\rho,\sigma}(1)P^{-1} = \phi^\dagger_{\bar\rho,\sigma}(1)$ with $\rho = -\bar\rho = +, -$ and $\sigma = \uparrow, \downarrow$. Its matrix representation is

$$P = \begin{pmatrix} 0 & 1 & 0 & 0\\ 1 & 0 & 0 & 0\\ 0 & 0 & 0 & 1\\ 0 & 0 & 1 & 0 \end{pmatrix} \tag{37}$$

in the basis set (35). Therefore, four eigenvectors have even or odd parity, i.e.,

$$\begin{aligned} &P|\psi_1\rangle = |\psi_1\rangle,\quad P|\psi_2\rangle = -|\psi_2\rangle,\\ &P|\psi_3\rangle = -|\psi_3\rangle,\quad P|\psi_4\rangle = |\psi_4\rangle, \end{aligned} \tag{38}$$

where the eigenvalues and eigenvectors are

$$\begin{aligned} &\varepsilon_2 = U_{\rm eff},\quad \varepsilon_3 = 0,\\ &\varepsilon_{1,4} = \frac{1}{2}(U_{\rm eff} \pm \sqrt{U_{\rm eff}^2 + 16J_{\rm eff}^2}), \end{aligned} \tag{39}$$

and

$$\begin{aligned} &|\psi_2\rangle = 2^{-1/2}(-1\ 1\ 0\ 0)^{\rm T},\\ &|\psi_3\rangle = 2^{-1/2}(0\ 0\ -1\ 1)^{\rm T},\\ &|\psi_{1,4}\rangle = (8 + 2|\varepsilon_{4,1}|^2)^{-1/2}(-2\ -2\ \varepsilon_{4,1}\ \varepsilon_{4,1})^{\rm T}. \end{aligned} \tag{40}$$

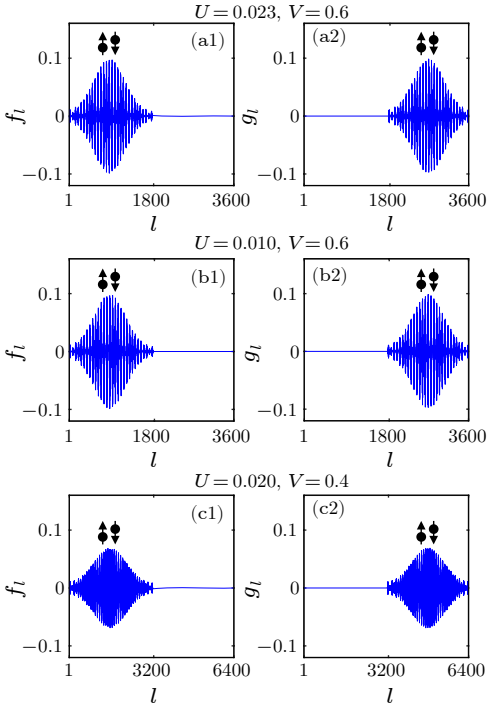

Fig. 5. Profiles of the initial and target states in Eq. (45), the coefficients f_l and g_l with $\kappa = \kappa_0$, obtained by exact diagonalization. Plots of f_l in (a1)–(c1) and g_l in (a2)–(c2) for three typical situations. The system parameters are $n_0 = 30$, $U = 0.023$, $V = 0.6$ in (a1) and (a2), $n_0 = 30$, $U = 0.010$, $V = 0.6$ in (b1) and (b2), $n0 = 40$, $U = 0.020$, $V = 0.4$ in (c1) and (c2), and $\kappa = 1$.

This system allows a special dynamics if we take

$$U_{\rm eff} = 2\Delta/(2\nu+1) = 4J_{\rm eff}/\sqrt{(2\nu+1)(2\nu+3)}, \tag{41}$$

at which we simply have

$$\varepsilon_1 = \left(\frac{2\nu+3}{2\nu+1}\right)\Delta,\ \varepsilon_2 = \frac{2}{2\nu+1}\Delta,\ \varepsilon_3 = 0,\ \varepsilon_4 = -\Delta, \tag{42}$$

where $\nu = 0, 1, 2, \ldots$. Such a commensurate energy level structure, together with the parities of the eigenvectors, allows the time evolution operator $\mathcal{U}(t) = e^{-ih_1t}$ to obey the connection to the parity operator

$$\mathcal{U}(t_q) = (-P)^q \tag{43}$$

at instant $t_q = q(2\nu+1)\pi/\Delta$. An arbitrary initial state can evolve naturally to its parity counterpart or itself periodically. For example, a Hubbard-pair initial state $\phi^\dagger_{+,\uparrow}(1)\phi^\dagger_{+,\downarrow}(1)|0\rangle$ can evolve to another Hubbard-pair state $\phi^\dagger_{-,\uparrow}(1)\phi^\dagger_{-,\downarrow}(1)|0\rangle$, realizing pair tunneling.

We investigate the tight-binding approximation by numerical simulation of the dynamics in the original system

with Eq. (1). We consider the Hamiltonian of a single Moiré unit cell,

$$H_{M1} = \sum_{j=1,\sigma=\uparrow,\downarrow}^{2n_0} \Big[-\kappa c^{\dagger}_{j,\sigma} c_{j+1,\sigma} + \text{H.c.} + (-1)^j V \times \cos\left(\frac{\pi j}{n_0}\right) n_{j,\sigma} \Big] + U \sum_{j=1}^{2n_0} n_{j,\uparrow} n_{j,\downarrow} + \kappa_0 \sum_{\sigma=\uparrow,\downarrow} (c^{\dagger}_{n_0,\sigma} c_{n_0+1,\sigma} + \text{H.c.}), \quad (44)$$

where the κ_0 term controls the connection between two halves of the chain: when taking $\kappa_0 = \kappa$, we have $J_{\text{eff}} = 0$. The computation is performed in two-particle subspace, where two particles have opposite spins. The subspace is spanned by a set of basis $\{c^{\dagger}_{i,\uparrow} c^{\dagger}_{j,\downarrow}|0\rangle,\ i, j = 1, \ldots, 2n_0\}$ of $(2n_0)^2$ dimensions.

We compute the initial state $|\psi_{\text{I}}\rangle$ and target state $|\psi_{\text{T}}\rangle$ by the exact diagonalization method for the system of Eq. (44) with $\kappa_0 = \kappa$. The initial state $|\psi_{\text{I}}\rangle$ and target state $|\psi_{\text{T}}\rangle$ has the form

$$|\psi_{\text{I}}\rangle = \sum_{l} f_l c^{\dagger}_{i,\uparrow} c^{\dagger}_{j,\downarrow}|0\rangle, \quad |\psi_{\text{T}}\rangle = \sum_{l} g_l c^{\dagger}_{i,\uparrow} c^{\dagger}_{j,\downarrow}|0\rangle, \quad (45)$$

where $l = 2n_0(i-1) + j$. Two states $|\psi_{\text{I}}\rangle$ and $|\psi_{\text{T}}\rangle$ are mutual parity counterparts due to the symmetry of H_{M1}. Taking $\kappa_0 = 0$, $|\psi_{\text{I}}\rangle$ can be set as an initial state for time evolution and $|\psi_{\text{I}}\rangle$ changes to $|\psi_{\text{T}}\rangle$ with a sufficiently long evolution time. Proper parameters (U and V) are searched to achieve the commensurate energy level structure as in Eq. (42). We plot the schematic illustration of the initial state $|\psi_{\text{I}}\rangle$ and target state $|\psi_{\text{T}}\rangle$ for three typical conditions (see Fig. 5). Obviously, the initial state $|\psi_{\text{I}}\rangle$ and target state $|\psi_{\text{T}}\rangle$ are mutual parity counterparts. The time evolution is computed for $\kappa_0 = 0$ by the formula

$$|\psi(t)\rangle = \exp(-iH_{1M}t)|\psi_{\text{I}}\rangle. \quad (46)$$

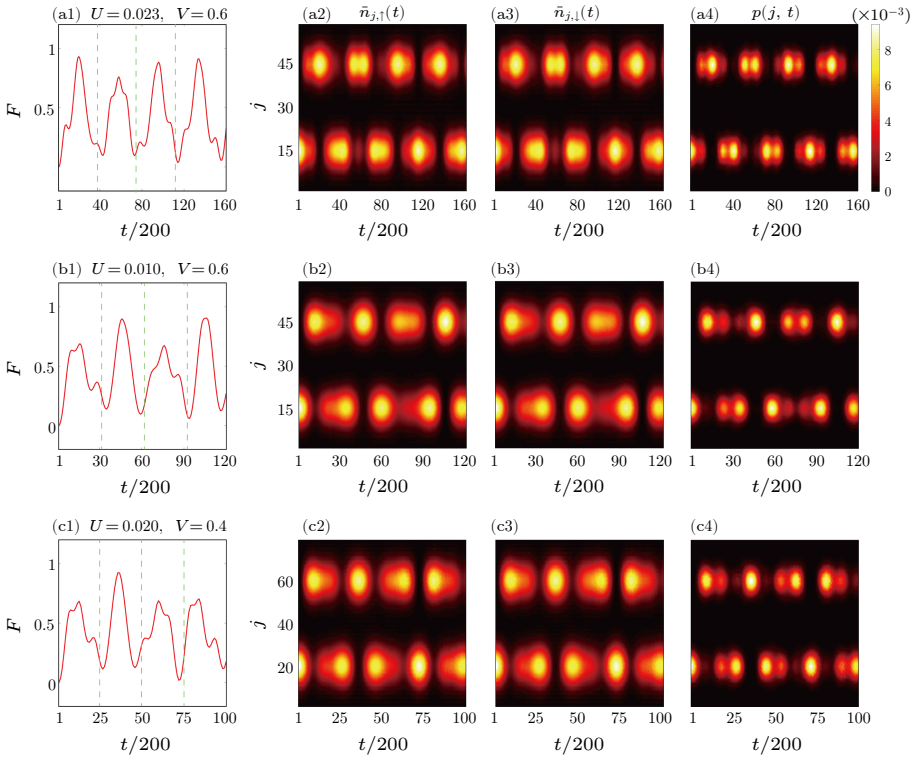

Fig. 6. Numerical results for the dynamical process of pair tunneling, obtained by exact diagonalization. Four quantities, (a1)–(c1) fidelity F, (a2)–(c2) $\overline{n}_{j,\uparrow}(t)$, (a3)–(c3) $\overline{n}_{j,\downarrow}(t)$, and (a4)–(c4) $p(j, t)$, defined in Eq. (47) are plotted for the evolved states in systems with four typical parameters. We determine that F, $\overline{n}_{j,\uparrow}$, $\overline{n}_{j,\downarrow}$, and p oscillate approximately with the period indicated by green dotted lines in (a1)–(c1), obtained from the analytical expression $T = 2\pi/\Delta$. Although the fidelity is not perfect, the pair tunneling is evident. The results indicate that the tight-binding approximation works quite well and a bound pair can be near perfectly transferred between two unit cells of a superlattice. The system parameters are $n_0 = 30$, $\Delta = 8.3 \times 10^{-4}$, $U = 0.023$, $V = 0.6$ in (a1)–(a4), $n_0 = 30$, $\Delta = 1.1 \times 10^{-3}$, $U = 0.010$, $V = 0.6$ in (b1)–(b4), and $n0 = 40$, $\Delta = 1.3 \times 10^{-3}$, $U = 0.020$, $V = 0.4$ in (c1)–(c4). The time unit is κ^{-1} and we take $\kappa = 1$.

We define four quantities

$$\begin{aligned} F(t) &= |\langle\psi_{\text{T}}|\psi(t)\rangle|, \\ \overline{n}_{j,\uparrow}(t) &= \langle\psi(t)|n_{j,\uparrow}|\psi(t)\rangle, \\ \overline{n}_{j,\downarrow}(t) &= \langle\psi(t)|n_{j,\downarrow}|\psi(t)\rangle, \\ p(j,\, t) &= \langle\psi(t)|n_{j,\uparrow}n_{j,\downarrow}|\psi(t)\rangle, \end{aligned} \quad (47)$$

to clarify our dynamical method. We plot these quantities for three typical conditions in Fig. 6. The numerical results indicate that a pair of electrons can nearly perfectly oscillate between two effective sites of one unit cell with different periods. Here, the numerical simulation is only performed for the case of $\nu = 0$, which corresponds to

$U_{\rm eff}/J_{\rm eff} = 2.309$ from Eq. (41). This ratio is much larger than $U/\kappa = 0.010$–0.023 indicated in Fig. 6. The numerical results illustrate that a spatially periodic external field really plays an important role in enhancing the correlation effect. The setting of system parameters is expected to provide guidance for the experiment.

In summary, we have demonstrated that the band structure of a simple one-dimensional Hubbard model can be constructed by applying a commensurate external field. Such a Moiré Hubbard model has a midgap flat band for zero U. The midgap physics can be well described by an effective Hubbard model when a weak U is switched on. The effective strengths of hopping and Hubbard interaction are controlled by the amplitude and period of the external field. This makes it possible to observe strongly correlated behaviors in a weak correlated system by adding a proper spatially periodic external field. Numerical simulations are performed for the finite-sized Moiré Hubbard system to demonstrate the validity of this approach. (i) We demonstrate that there exists a set of bound-pair energy levels, including the η-pairing state. It indicates that the tight-binding approximation works well. (ii) We further present the phenomenon of bound-pair oscillation, which reveals the dynamics occurring in a Moiré Hubbard system with relatively strong correlation. The phenomenon of oscillation indicates that the on-site Hubbard interaction in the unit of hopping strength can be enhanced by more than 2 orders. This work provides a method to enhance the correlated effect by the spatially periodic external field and is expected to provide guidance for the experiment.

Acknowledgement. This work was supported by the National Natural Science Foundation of China (Grant Nos. 12305026 and 12374461).

References

[1] Bistritzer R and MacDonald A H 2011 *Proc. Natl. Acad. Sci. USA* **108** 12233
[2] Cao Y, Luo J Y, Fatemi V, Fang S, Sanchez-Yamagishi J D, Watanabe K, Taniguchi T, Kaxiras E, and Jarillo-Herrero P 2016 *Phys. Rev. Lett.* **117** 116804
[3] Cao Y, Fatemi V, Demir A, Fang S, Tomarken S L, Luo J Y, Sanchez-Yamagishi J D, Watanabe K, Taniguchi T, Kaxiras E, Ashoori R C, and Jarillo-Herrero P 2018 *Nature* **556** 80
[4] Cao Y, Fatemi V, Fang S, Watanabe K, Taniguchi T, Kaxiras E, and Jarillo-Herrero P 2018 *Nature* **556** 43
[5] Kim K, DaSilva A, Huang S Q, Fallahazad B, Larentis S, Taniguchi T, Watanabe K, LeRoy B J, MacDonald A H, and Tutuc E 2017 *Proc. Natl. Acad. Sci. USA* **114** 3364
[6] Yankowitz M, Chen S W, Polshyn H, Zhang Y X, Watanabe K, Taniguchi T, Graf D, Young A F, and Dean C R 2019 *Science* **363** 1059
[7] Lu X B, Stepanov P, Yang W, Xie M, Aamir M A, Das I, Urgell C, Watanabe K, Taniguchi T, Zhang G Y, Bachtold A, MacDonald A H, and Efetov D K 2019 *Nature* **574** 653
[8] Shen C, Ying J H, Liu L *et al.* 2021 *Chin. Phys. Lett.* **38** 047301
[9] Zhang X, Pan G, Zhang Y, Kang J, and Meng Z Y 2021 *Chin. Phys. Lett.* **38** 077305
[10] Li X F, Sun R X, Wang S Y, Li X, Liu Z B, and Tian J G 2022 *Chin. Phys. Lett.* **39** 037301
[11] Ma J J, Wang Z Y, Xu S G, Gao Y X, Zhang Y Y, Dai Q, Lin X, Du S X, Ren J, and Gao H J 2022 *Chin. Phys. Lett.* **39** 047403
[12] Wang Y, Liu Y, Hao Z *et al.* 2023 *Chin. Phys. Lett.* **40** 049901
[13] Chen X T, Liu C H, Xu D H, and Chen C Z 2023 *Chin. Phys. Lett.* **40** 097403
[14] Dong S J, Zhang H, Wang C, Zhang M, Han Y J, and He L X 2023 *Chin. Phys. Lett.* **40** 126403
[15] Wu H C, Xu H S, Xie L C, and Jin L 2024 *Phys. Rev. Lett.* **132** 083801
[16] Xie L C, Jin L, and Song Z 2023 *Sci. Bull.* **68** 255
[17] Yankowitz M, Xue J, Cormode D, Sanchez-Yamagishi J D, Watanabe K, Taniguchi T, Jarillo-Herrero P, Jacquod P, and LeRoy B J 2012 *Nat. Phys.* **8** 382
[18] Ponomarenko L A, Gorbachev R V, Yu G L, Elias D C, Jalil R, Patel A A, Mishchenko A, Mayorov A S, Woods C R, Wallbank J R, Mucha-Kruczynski M, Piot B A, Potemski M, Grigorieva I V, Novoselov K S, Guinea F, Fal'ko V I, and Geim A K 2013 *Nature* **497** 594
[19] Dean C R, Wang L, Maher P, Forsythe C, Ghahari F, Gao Y, Katoch J, Ishigami M, Moon P, Koshino M, Taniguchi T, Watanabe K, Shepard K L, Hone J, and Kim P 2013 *Nature* **497** 598
[20] Hunt B, Sanchez-Yamagishi J D, Young A F, Yankowitz M, LeRoy B J, Watanabe K, Taniguchi T, Moon P, Koshino M, Jarillo-Herrero P, and Ashoori R C 2013 *Science* **340** 1427
[21] Woods C R, Britnell L, Eckmann A, Ma R S, Lu J C, Guo H M, Lin X, Yu G L, Cao Y, Gorbachev R V, Kretinin A V, Park J, Ponomarenko L A, Katsnelson M I, Gornostyrev Y N, Watanabe K, Taniguchi T, Casiraghi C, Gao H J, Geim A K, and Novoselov K S 2014 *Nat. Phys.* **10** 451
[22] Nakajima S, Tomita T, Taie S, Ichinose T, Ozawa H, Wang L, Troyer M, and Takahashi Y 2016 *Nat. Phys.* **12** 296
[23] Lohse M, Schweizer C, Zilberberg O, Aidelsburger M, and Bloch I 2016 *Nat. Phys.* **12** 350
[24] Wang R, Wang P, Zhang K L, and Song Z 2020 *Phys. Rev. B* **102** 094207
[25] Wang R, Yang X M, and Song Z 2021 *J. Phys.: Condens. Matter* **33** 365403
[26] Yang X M, Zhang X Z, Li C, and Song Z 2018 *Phys. Rev. B* **98** 085306
[27] Tasaki H 1998 *J. Phys. C* **10** 4353
[28] Essler F H L, Frahm H, Gohmann F, Klumper A, and Korepin V E 2005 *The One-Dimensional Hubbard Model* (Cambridge: Cambridge University Press)
[29] Jin L, Chen B, and Song Z 2009 *Phys. Rev. A* **79** 032108
[30] Jin L and Song Z 2011 *Phys. Rev. A* **83** 052102
[31] Yang C N 1989 *Phys. Rev. Lett.* **63** 2144
[32] Corrielli G, Crespi A, Della Valle G, Longhi S, and Osellame R 2013 *Nat. Commun.* **4** 1555